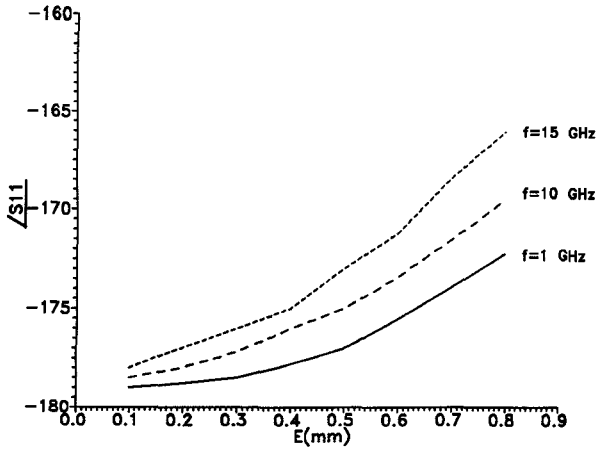


Fig. 3. Variation of $\angle S_{11}$ with respect to the eccentricity.

10 GHz and 15 GHz. Notice that strong reflections are observed as the eccentricity becomes comparable to the microstrip line widths.

## V. Conclusions

A frequency-dependent analysis of the shielded microstrip asymmetric step discontinuity has been presented. The asymmetric nature of the discontinuity requires the investigation of the spectrum of both odd and even hybrid modes. Numerical results have been presented and the effect of the eccentricity on the scattering parameters has been depicted. In principal the same method can be employed to treat other types of asymmetric discontinuity problems.

## References

[1] N. H. L. Koster and R. H. Jansen, "The microstrip step discontinuity: a revised description," *IEEE Trans. Microwave Theory Tech.*, vol. MTT-34, pp. 213–222, 1986.

[2] T. Chu and T. Itoh, "Generalized scattering matrix method for analysis of cascaded and offset microstrip step discontinuities," *IEEE Trans. Microwave Theory Tech.*, vol. MTT-34, pp. 280–284, Feb. 1986.

[3] Benedek and P. Sylvester, "Equivalent capacitances for microstrip gaps and steps," *IEEE Trans. Microwave Theory Tech.*, vol. MTT-20, pp. 729–733, 1972.

[4] A. F. Thomson and A. Gopinath, "Calculation of microstrip discontinuity inductances," *IEEE Trans. Microwave Theory Tech.*, vol. MTT-23, pp. 177–179, 1972.

[5] G. Kompa, "Design of stepped microstrip components," *Radio Electron. Eng.*, vol. 48, pp. 53–63, 1978.

[6] R. H. Jansen, "The spectral domain approach for microwave integrated circuits," *IEEE Trans. Microwave Theory Tech.*, vol. MTT-33, pp. 1043–1056, 1985.

[7] T. S. Chu, T. Itoh, and Yi Chi Shih, "Comparative study of mode matching formulations for microstrip discontinuity problems," *IEEE Trans. Microwave Theory Tech.*, vol. MTT-33, pp. 1018–1023, 1985.

[8] R. K. Hoffman, *Integrierte Mikrowellenshcaltungen.* Berlin: Springer-Verlag, 1983.

[9] K. C. Gupta, R. Garg, and I. J. Bahl, *Microstrip Lines and Slotlines.* Dedham, MA: Artech House, 1979 sec. 3.4.3.

[10] K. C. Gupta, R. Garg, and R. Chadha, *Computer Aided Design of Microwave Circuits.* Dedham, MA: Artech House, 1981 sec. 6.2.4.

[11] T. C. Edwards, *Foundations for Microstrip Circuit Design.* ch. 5, New York: Wiley, 1981.

[12] R. Mehran, *Grundelemente des rechnergestutzen Entwurfs von Mikrostreifenleitungs-Schaltungen.* Aachen: Verlag. H. Wolff, 1983.

[13] R. Mittra and T. Itoh, "A new technique for the analysis of the dispersion characteristics of microstrip lines," *IEEE Trans. Microwave Theory Tech.*, vol. MTT-19, pp. 47–56, 1971.

[14] N. Uzunoglu, C. Capsalis, and C. Chronopoulos, "Frequency dependent analysis of a shielded microstrip step discontinuity using an efficient mode-matching technique," *IEEE Trans. Microwave Theory Tech.*, vol. 36, pp. 976–984, 1988.

[15] J.-T. Kuo and C.-K. C. Tzang, "Complex modes in shielded suspended coupled microstrip lines," *IEEE Trans. Microwave Theory Tech.*, vol. 38, pp. 1278–1286, Sept. 1990.

[16] S. Omar and K. Schuenemann, "The effect of complex modes at finline discontinuities," *IEEE Trans. Microwave Theory Tech.*, vol. MTT-34, pp. 1508–1514, Dec. 1986.

# Semi-Discrete Finite Element Analysis of Zero-Thickness Inductive Strips in a Rectangular Waveguide

Devin Crawford and Marat Davidovitz

***Abstract*—A semi-discrete finite element method is applied to determine the network parameters for zero-thickness inductive discontinuities in a rectangular guide. The solution obtained is computationally efficient and is applicable under multi-mode conditions. Moreover, after obtaining the solution for a given geometry at a specific frequency, further frequency analysis for the same geometry requires only nominal additional recalculation. Convergence properties of the solution are studied and comparison with published data is carried out to verify the solution accuracy.**

## I. Introduction

A variant of the FEM, the Semi-Discrete Finite Element Method (SDFEM) utilizes the properties of the FEM in one plane of the domain, while the solution along the remaining dimension is found analytically. Thus, the computational burden associated with this method is considerably smaller than that for a fully-discrete FEM solution. Moreover, in the framework of the SDFEM, radiation condition can be rigorously applied along certain directions in a Cartesian coordinate system. Therefore, the SDFEM is suited to problems involving discontinuities in a plane. Here we examine the problem of zero-thickness inductive discontinuities in a waveguide. This problem has been extensively studied in the past [1], [2], [3], [4], [7], and therefore is a good model problem with which to verify the proposed method, as well as examine its characteristics in detail.

Section II of this paper deals with the theoretical formulation of the problem, based on the scalar Helmholtz equation for the TE field. In Section III the numerical issues of discretization, convergence and execution time are examined. In section IV, we compare our results with published data [7] and finally, Section V contains conclusions and suggestions for further work.

## II. Formulation of the Problem

Consider a general, infinitesimally thin inductive diaphragm shown in Fig. 1. It is assumed that the $TE_{10}$ mode is incident from $z < 0$. It is well-known [5] that for this type of discontinuity only higher-order $TE_{n0}$ modes are excited. Therefore the scattered TE field satisfies the

Manuscript received February 4, 1992; revised June 30, 1992.

The authors are with the Department of Electrical Engineering, University of Minnesota, 200 Union Street SE, Minneapolis, MN 55455.

IEEE Log Number 9205466.

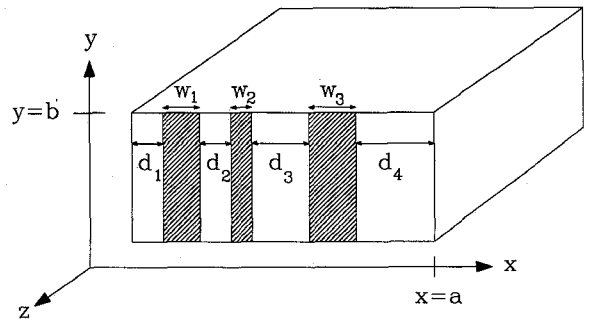


Fig. 1. Description of the problem geometry.

following scalar Helmholtz equation

$$\left(\frac{\partial^2}{\partial x^2}+\frac{\partial^2}{\partial z^2}\right)\phi(x,z) + k^2\phi(x,z) = j\omega\mu J_y(x)\delta(z) \tag{1}$$

where $\phi(x,z)$ denotes the $y$ component of the reflected electric field, and $J_y(x)$ is the current induced on the discontinuity by the incident wave.

The finite element method is used to discretize the field equations in the plane transverse to the direction of propagation in the waveguide. Since the field is independent of $y$, only 1-dimensional discretization along the $x$ axis is necessary. The dependence of the solution along the $z$ direction will be determined analytically.

The following boundary conditions will be applied to the Helmholtz equation at various stages of the formulation

$$\phi(x,z) = 0; x = 0, a \tag{2}$$

$$\phi(x,z) = -\sin\left(\frac{\pi x}{a}\right)\forall(x,z)\in\mathcal{S} \tag{3}$$

where $\mathcal{S} = \cup_i \mathcal{S}_i$, and $\mathcal{S}_i$ is the surface of the $i$th conducting strip. Equation (3) simply imposes the condition requiring the sum of the incident and reflected fields to vanish on the diaphragm.

Multiplying (1) by a weight function $\psi(x)$ and integrating over the cross-section, (1) can be expressed in its weak form [8] [9] as follows

$$\int_0^a \left[\left(\frac{\partial^2}{\partial x^2}+\frac{\partial^2}{\partial z^2}\right)\phi(x,z) + k^2\phi(x,z)\right]\psi(x)\,dx = \int_0^a j\omega\mu J_y(x)\delta(z)\psi(x)\,dx \tag{4}$$

Equation (4) will serve as the basis for construction of the SDFEM solution. For reasons that will become apparent shortly, it is convenient to alter (4) through integration by parts

$$\int_0^a \left[\frac{\partial^2\phi}{\partial z^2} - \frac{\partial\phi}{\partial x}\frac{\partial\psi}{\partial x} + k^2\phi\psi\right]\cdot dx + \frac{\partial\phi}{\partial x}\psi\Big|_0^a = \int_0^a j\omega\mu J_y(x)\delta(z)\psi\,dz \tag{5}$$

In the finite element nomenclature this equation constitutes the weak, symmetric form of the original differential formulation. The name stems from the symmetry between the unknown $\phi$ and the weight function $\psi$ in the discretized portion of the domain.

The finite element solution can be written in terms of a set of basis functions $\{\phi_p(x), p = 0, N+1\}$ which span the $x$-domain. The basis functions are defined piecewise by low-order polynomials over a mesh, and are normalized so that $\phi_p(x_q) = \delta_{pq}$, where $\delta_{pq}$ is the Kronecker delta, and $x_q$ is the $x$ position corresponding to node $q$.

An approximate solution can be expressed in terms of the basis functions as

$$\phi(x,z) = \sum_{q=0}^{N+1} v_q(z)\phi_q(x) = \tilde{\boldsymbol{\phi}}(x)\boldsymbol{v}(z) \tag{6}$$

where

$v_q(z)$-value of the F.E.M. solution at $(x_q, z)$,

$\phi_q(x)$-the $q$-th basis function,

$\phi(x)$-the vector whose elements are $\phi_q(x)$,

$\boldsymbol{v}(z)$-the vector whose elements are $v_q(z)$, and tilda denotes transposition.

We will also take

$$\psi(x) = \phi_q(x), p = 0, 1, 2, \cdots, N+1 \tag{7}$$

Application of the essential boundary conditions of (2) requires that

$$v_0(z) = v_{N+1}(z) = 0$$

eliminating the term $(\partial\phi/\partial x)\psi|_0^a$ in (5).

Substitution of expressions (6) and (7) into (5) yields the following matrix equation

$$\boldsymbol{B}\left(\frac{d^2v(z)}{dz^2} + k^2\boldsymbol{v}(z)\right) - \boldsymbol{A}\boldsymbol{v}(z) = \delta(z)\boldsymbol{s} \tag{8}$$

where $\boldsymbol{A}$ and $\boldsymbol{B}$ are $N \times N$ matrices, and $\boldsymbol{s}$ is a vector whose elements are defined as follows:

$$a_{pq} = \int_0^a \frac{d\phi_p}{dx}\frac{d\phi_q}{dx}dz \tag{9}$$

$$b_{pq} = \int_0^a \phi_p(x)\phi_q(x)\,dx \tag{10}$$

$$s_p = \int_0^a j\omega\mu J_y(x)\phi_p(x)\,dx \tag{11}$$

The $N$ differential equations in the matrix equation (8) must now be decoupled. In order to accomplish this task, let the linear transformation matrix $\boldsymbol{T}$ be defined by

$$\boldsymbol{v}(z) \equiv \boldsymbol{T}\boldsymbol{V}(z) \tag{12}$$

where $\boldsymbol{V}$ denotes the transformed solution.

In order to decouple the equations, $\boldsymbol{T}$ must satisfy the generalized eigenvalue problem

$$\boldsymbol{A}\boldsymbol{T} = \boldsymbol{B}\boldsymbol{T}\boldsymbol{K} \tag{13}$$

where the diagonal matrix $\boldsymbol{K}$ has the eigenvalue entries $\lambda_p$. Transforming equation (8) to the principle axes yields the following $N$ uncoupled differential equations

$$\frac{d^2\boldsymbol{V}(z)}{dz^2} + k^2\boldsymbol{V}(z) - \boldsymbol{K}\boldsymbol{V}(z) = \delta(z)\hat{\boldsymbol{s}} \tag{14}$$

where

$$\boldsymbol{s} = \boldsymbol{T}^{-1}\boldsymbol{B}^{-1}\boldsymbol{s} \tag{15}$$

and $k^2 = \omega^2\mu\epsilon$.

After solving the equations and applying the radiation conditions at $z \approx \pm\infty$, we can express $\boldsymbol{V}(z)$ as

$$\boldsymbol{V} = \hat{\boldsymbol{Z}}(z)\hat{\boldsymbol{s}} \tag{16}$$

where $\hat{\boldsymbol{Z}}(z)$ is a diagonal matrix with elements

$$\hat{Z}_{pp} = \frac{-e^{-\gamma_p|z|}}{2\gamma_p} \tag{17}$$

and

$$\gamma_p \equiv \sqrt{\lambda_p - k^2} \tag{18}$$

If the transformation matrix $\boldsymbol{T}$ is normalized such that $\tilde{\boldsymbol{T}}\boldsymbol{B}\boldsymbol{T} = \boldsymbol{I}$, then from (12), (15) and (16) it follows that

$$\boldsymbol{v}(z) = \boldsymbol{T}\hat{\boldsymbol{Z}}(z)\boldsymbol{T}^{-1}\boldsymbol{B}^{-1}\boldsymbol{s} = \boldsymbol{T}\hat{\boldsymbol{Z}}(z)\tilde{\boldsymbol{T}}\boldsymbol{s} \tag{19}$$

In order to express $\boldsymbol{v}(z)$ in a simple form, let $\boldsymbol{Z}(z) = \boldsymbol{T}\hat{\boldsymbol{Z}}(z)\tilde{\boldsymbol{T}}$. The boundary conditions stated in (3) can now be applied to solve for $\boldsymbol{s}$.

The boundary condition of eq. (3) is applied by defining the vector $\phi_o$ that has elements

$$\phi_{op}(x_p, 0) = \begin{cases} \sin(\pi x_p/a) & \text{if } x_p \in \mathcal{S} \\ 0 & \text{if } x_p \ni \mathcal{S} \end{cases} \tag{20}$$

Applying (6) and (19), and the definitions of $\boldsymbol{Z}(z)$ and $\phi_o$ to (3) we see that

$$-\phi_o = \boldsymbol{Z}(0)\boldsymbol{s} \tag{21}$$

which is actually a matrix equation in $M$ unknowns, where $M$ is the number of nodes in $\mathcal{S}$. The vector $\boldsymbol{s}$ can be determined by extracting from $\boldsymbol{Z}(0)$ the rows corresponding to the non-zero elements of $\phi_o$ and solving for the non-zero elements of $\boldsymbol{s}$. Once $\boldsymbol{s}$ is found, the value of the reflected field at any point $(x, z)$ can be determined by substituting $\boldsymbol{s}$ into (6) and (19)..

The reflection coefficient is extracted by projecting the finite element solution onto the $TE_{10}$ mode, yielding

$$\Gamma = \frac{\int_0^a \phi(x,0)\sin\left(\frac{\pi x}{a}\right)dx}{\int_0^a \sin^2\left(\frac{\pi x}{a}\right)dx}$$

Finally, we wish to model the discontinuity in terms of a lumped element, namely, as an inductor. From transmission line theory, the normalized susceptance is given by

$$j\bar{b} = -\frac{2\Gamma}{1+\Gamma} \tag{22}$$

The current on the strips can also be found by first expressing it as a linear combination of the same basis functions that were used to define the solution, that is

$$J_y(x) = \sum_{q=1}^{N} J_q \phi_q(x) \tag{23}$$

Substituting (23) into (11) gives

$$\int_0^a j\omega\mu J_y(x)\psi(x)\,dx = \sum_{p=1}^{N}\sum_{q=1}^{N} j\omega\mu J_q\left[\int_0^a \phi_p(x)\phi_q(x)\,dx\right] \tag{24}$$

and it follows from the definition of the matrix $\boldsymbol{B}$ in (10) that the vector $\boldsymbol{J}$ whose elements are $J(x_p)$ can be expressed as

$$\boldsymbol{s} = j\omega\mu\boldsymbol{B}\boldsymbol{J} \tag{25}$$

Since $J_p = 0$ if $x_p \ni \mathcal{S}$ the problem can be reduced to a set of independent matrix equations, with each set of equations corresponding to one strip.

## III. Numerical Considerations

In computing the data presented in this and the following section, the numerical solution outlined in the Section II was implemented using piecewise-linear basis functions in (6). The nodes defining the element boundaries along the $x$-axis were distributed non-uniformly, in a somewhat ad hoc manner, according to the following set of guidelines:

- The node distribution is governed by the local behavior of the solution, i.e. the regions of the $x$-axis where the solution and/or its derivatives vary rapidly or exhibit singularities must undergo fine discretization, while coarser meshes can be placed over the domain portions with slower solution variation. In finite element solutions employing low-order piecewise-polynomial basis functions the node placement around singularities is particularly important, since it ultimately determines the rate of convergence [6].
- In the semi-discrete approach, the finite element approximation is introduced only in the variable $x$. Therefore it is the $x$-variation of the solution which determines the node distribution.

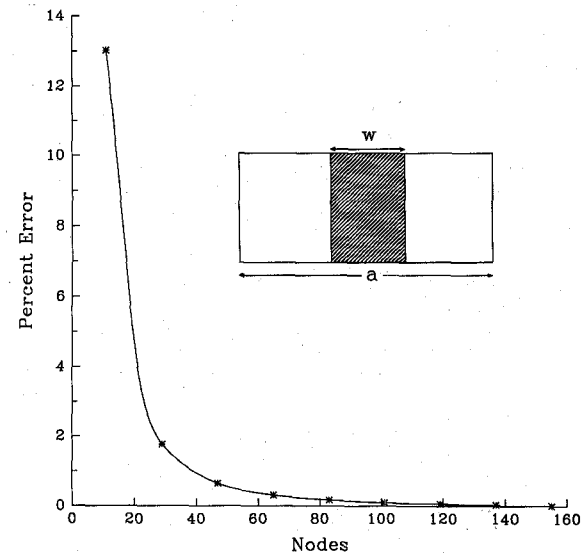


(a)

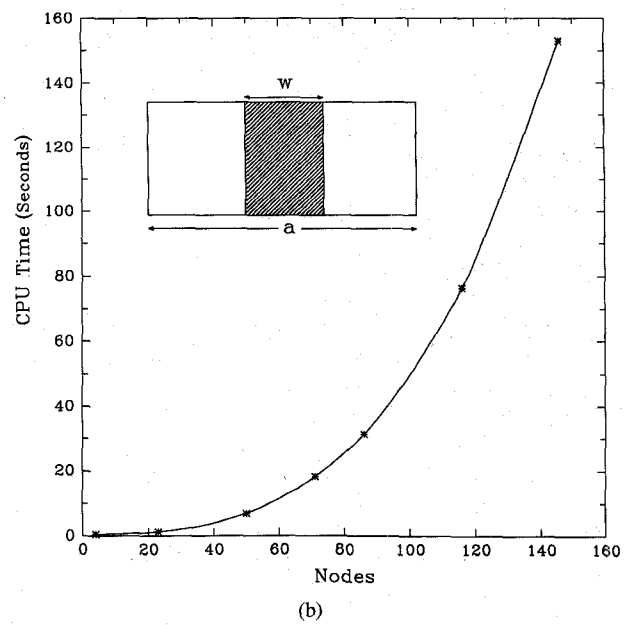


(b)

Fig. 2. (a) Convergence for the single centered strip. $(w/a = 0.2, \lambda/a = 1.25)$. (b) CPU time required to run the single strip problem. $(w/a = 0.2, \lambda/a = 1.25)$.

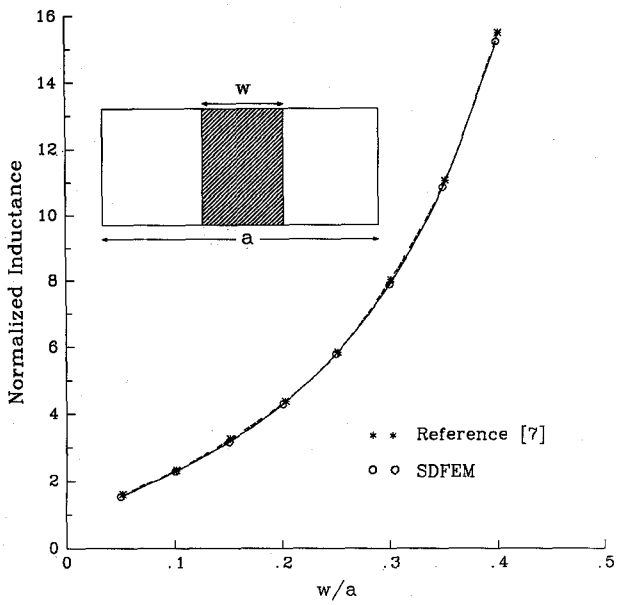


Fig. 3. Normalized inductance for the single centered strip as a function of strip width. $\lambda/a = 1.25$.

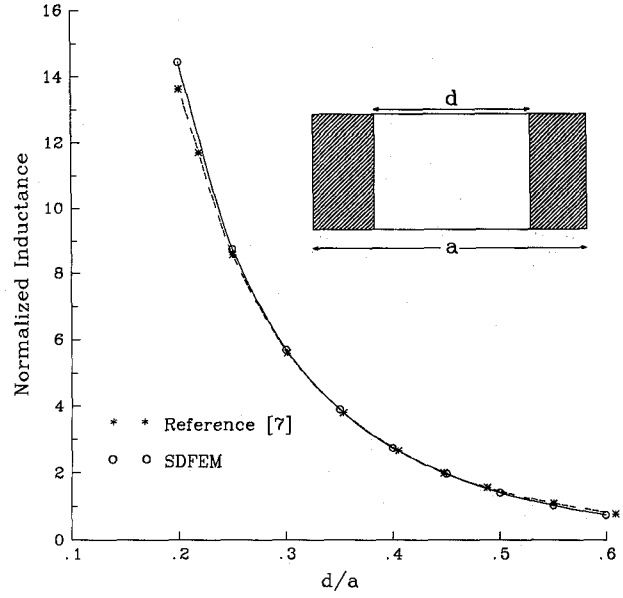


Fig. 4. Normalized inductance for the inductive window as a function of window size. $\lambda/a = 1.25$.

For the problem at hand, the most severe behavior in the solution occurs close to the edges of the strip discontinuities, where the first $x$ -derivative of the electric field parallel to the edge becomes singular in the manner dictated by the edge condition. Therefore, it is important to introduce a graded mesh in the vicinity of the strip edges.

- The construction of a non-uniform mesh on a given interval can be accomplished by introducing a *mesh-function*, i.e. a mapping from a uniform to a graded mesh. For the problem at hand a graded mesh was constructed by initially sub-dividing the $x$-domain $(0 < x < a)$ into intervals delimited by the strip edges. The discretization on each interval was carried out by means of the following mesh-function

$$x_{gr} = x_{cr} + \frac{\Delta x_r}{2} \cos^{\alpha} \frac{\pi q}{N_r}$$

where

$x_{qr}$-location of the $q$-th node on the $r$-th interval;

$x_{cr}, \Delta x_r$-center and length, respectively, of the $r$th interval;

$\alpha$-empirical exponent determined to optimize the convergence rate;

$N_r$ total number of nodes on the $r$th interval.

For the two interval adjacent to the waveguide lateral walls we set $x_c = 0, a$, since the solution is well behaved at $x = 0, a$.

Note, with the exception of the parameter $\alpha$, this meshing algorithm was employed in [10].

The rate of convergence for a model problem is illustrated in Fig. 2(b). Optimal convergence for this and subsequent calculations was obtained with $\alpha = 0.7$. A closer examination of the curve reveals that the rate of convergence is $O(1/N^2)$. In Fig. 2(a) the CPU time required to execute the model problem for a given number of mesh nodes is graphed. The machine used was a DecStation 3100 with 16Mb of RAM. Approximately 70% of the execution time was spent in solving the eigenvalue problem in (13).

## IV. Results

The normalized inductance calculated using the SDFEM is shown in Figs. 3–5 for three basic problems. The results are compared

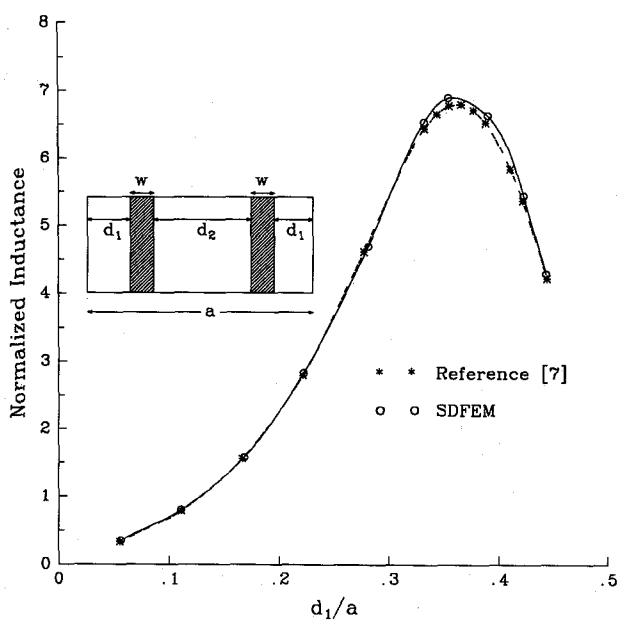


Fig. 5. Normalized inductance for two symmetrically located strips. $\lambda/a = 1.591, w/a = 0.055$.

with a moment method based numerical solution [7]. Clearly, the discrepancy between the solutions is minimal.

To verify the validity of the solution further, current distribution on the inductive strips was calculated using (25) and is shown in Fig. 6. Note that the singularity in the current distribution at the strip edges, which is expected on the basis of the edge condition, is captured in the numerical solution.

It is important to note that the eigenvalue problem of (13) depends only on the physical geometry of the waveguide and not on the frequency of the propagating mode. Therefore the frequency response of a waveguide can be calculated efficiently after having solved the bulk of the numerical problem, namely the eigenvalue equation (13), only once.

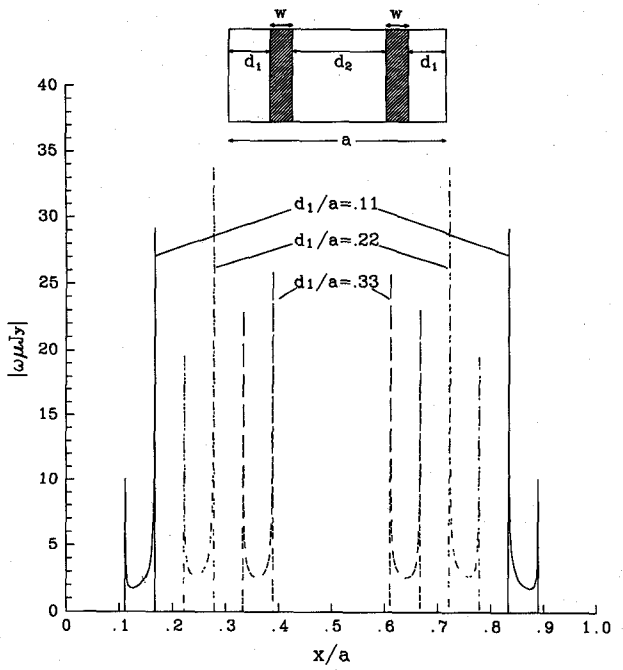


Fig. 6. Current distribution on two symmetrically located strips. $\lambda/a = 1.591$.

## V. Conclusions

We have illustrated the applicability of the SDFEM to a specific set of rectangular waveguide discontinuity problems. The numerical properties of the solution were studied and its accuracy verified. Further work in this area should now be done to apply the SDFEM to problems with thick and/or cascaded discontinuities in waveguides of arbitrary cross-section. In these cases the general $TM_{mn}$ and $TE_{mn}$ modes should be included in the analysis.

## References

[1] M. Guglielmi and C. Newport, "Rigorous, multimode equivalent network representation of inductive discontinuities," *IEEE Trans. Microwave Theory Tech.*, vol. 38, no. 11, pp. 1651–1659, Nov. 1990.

[2] H. Auda and R. F. Harrington, "Inductive posts and diaphragms of arbitrary shape and number in a rectangular waveguide," *IEEE Trans. Microwave Theory Tech.*, vol. MTT-32, no. 6, pp. 604–613, June 1984.

[3] K. Chang, "Impedance calculation of three narrow resonant strips on the transverse plane of a rectangular waveguide," *IEEE Trans. Microwave Theory Tech.*, vol. MTT-32, no. 1, pp. 126–130, Jan. 1984.

[4] N. Marcuvitz, *Waveguide Handbook*. Lexington, MA: Boston Technical Publishers, 1964.

[5] R. E. Collin, *Field Theory of Guided Waves*. New York: McGraw-Hill, 1960.

[6] E. B. Becker, G. F. Carey, and J. T. Oden, *Finite Elements: An Introduction*. Englewood Cliffs, NJ: Prentice-Hall, 1981.

[7] S. N. Sinah, "Analysis of multiple-strip discontinuity in a rectangular waveguide," *IEEE Trans. Microwave Theory Tech.*, vol. MTT-34, no. 6, June 1986.

[8] M. Davidovitz and Z. Wu, "Semi-discrete finite element method analysis of microstrip structures," in *Directions in Electromagnetic Wave Modeling*, H. L. Bertoni and L. B. Felsen, Eds. New York: Plenum Press, 1991.

[9] M. Davidovitz, "Calculation of multiconductor mictrostrip line capacitances using the semidiscrete finite element method," *IEEE Microwave Guided Wave Lett.*, vol. 1, no. 1, pp. 5–7, Jan. 1991.

[10] H. Diestel, "Analysis of planar multiconductor transmission lines with the method of lines," *AEÜ*, vol. 41, pp. 169–175, 1987.

# Accurate and Efficient Computation of Dielectric Losses in Multi-Level, Multi-Conductor Microstrip For CAD Applications

James P. K. Gilb and Constantine A. Balanis

***Abstract*— Accurate and efficient computation of dielectric losses in complex microstrip structures is important in the computer-aided design of microwave and millimeter-wave integrated circuits. The proposed approach can be used in lieu of lossy, full-wave solutions to provide accurate and efficient data for the CAD of multi-level, multi-conductor MIC and MMIC structures. This new application gives results that are as accurate as lossy full-wave techniques over a wide range of frequencies, including the dispersive region. In addition to providing accurate results, this method is up to three times faster, depending on the number and type of substrates or superstrates. Results are shown for various multi-conductor, multi-level structures which compare well with the lossy, full-wave approach and require significantly less computer time.**

## I. Introduction

One of the most important goals in the computer modeling of MIC's and MMIC's is to provide highly accurate simulations in order to reduce the number of design iterations. Accurate modeling of all of the characteristics of multi-level, multi-conductor structures is necessary in the quest for single iteration design of complex circuits. At the same time, to facilitate the design process, these accurate methods must also provide results as quickly as possible. Current techniques available for the calculation of the dielectric attenuation coefficient compromise on either accuracy or speed, and many are not suitable for complex structures. In addition, lossy full-wave techniques usually require completely different subroutines and utility libraries. A new application of an old formulation is presented here which provides accurate results for the dielectric loss coefficient for multi-level, multi-conductor structures in about one-third the time required for a lossy, full-wave computation. This new approach is ideally suited for CAD applications since it uses currently available lossless techniques and does not require special subroutines and software libraries.

Various full-wave methods have been used to compute the dielectric loss in multi-layer, multi-conductor structures. The Spectral Domain Approach (SDA) has been used, both with a perturbational formula for the attenuation coefficient [1] and by formulating the problem with a complex dielectric constant [2]–[4]. Other full-wave techniques that have been used include the space-domain, moment method [5], and the Finite-Difference Time-Domain (FDTD) [6]. All of these techniques give accurate results for the dielectric loss in a general microstrip structure, but they require a significant amount of computational effort. An alternate approach is to use an approximate formula for the dielectric loss coefficient. One of the most widely used formulas for computing the dielectric attenuation coefficient is the one advanced by Schneider [7]. This formula has long been used with approximate formulas for $\epsilon_{reff}$ to compute the dielectric attenuation coefficient, $\alpha_d$. It was recently shown that this formula gives results that are as accurate as those obtained with a lossy

Manuscript received February 4, 1992; revised June 22, 1992. This work was partially supported by the U.S. Army Research Office under grant DAAL03-92-G-0262.

The authors are with the Department of Electrical Engineering, Telecommunications Research Center, Arizona State University, Tempe, AZ 85287-7206.

IEEE Log Number 9205467.